P2.13 Comparing snowstorms with and without lightning via the growth rate parameter

Christopher J. Melick*, Brian P. Pettegrew, Larry L. Smith+, Amy E. Becker, Patrick S. Market, and Anthony R. Lupo

Department of Soil, Environmental, and Atmospheric Science
University of Missouri-Columbia
Columbia, MO

1. INTRODUCTION

Curran and Pearson (1971) were among the first to investigate the regular occurrence of snow with thunder across the United States. Their study along with others (e.g., Holle and Cortinas 1998; Market et al. 2002) indicated a tendency for such events to occur over specific geographical regions, the central United States repeatedly being one of those preferred locations. Unlike the more easily identifiable surface influences, such as orographic and lake-effect processes (Schultz 1999), many cases of convective snowfall result from the release of elevated instability within the much larger circulation pattern of extratropical cyclones (ETC; Market et al. 2002; Market et al. 2006).

The work presented here examines the stability characteristics of thundersnow events immediately prior to initiation. In order to accomplish this objective for the winter seasons of 2003-04 and 2004-05 (October-April), calculations of a growth rate parameter (σ^2) from numerical weather model output will be utilized. In the past, values of σ^2 have been applied as a proxy to evaluate the presence of mesoscale precipitation banding (Bennetts and Sharp 1982). This particular approach has been accomplished for the same set of convective snow case studies recently by Melick et al. (2007). For the current work, growth rates are examined as to whether destabilization of the environment over a relatively short period of time can be diagnosed in conjunction with the use of 3-D equivalent potential vorticity (EPV; McCann 1995). A collection of non-thundering snowstorms was included to highlight the importance of the results when lightning was present. Finally, trends in a traditional stability index (mid-level lapse rates) will be examined to support results from σ^2.

* **Corresponding author**: Christopher J. Melick, University of Missouri-Columbia, 302 Anheuser-Busch Natural Resources Building, Columbia, MO 65211. E-mail: cjmzr5@mizzou.edu

+ **Current Affiliation:** Larry L. Smith, National Weather Service Office, 4003 Cirrus Drive, Medford, OR 97504-4198. E-mail: Larry.Smith@noaa.gov

2. STABILITY PARAMETERS

Narrow lines of clouds and precipitation are often found in the vicinity of frontal systems. In order to explain the origin of these banded features, Bennetts and Hoskins (1979) revealed evidence through numerical modeling and observations that conditional symmetric instability (CSI) might be an important mechanism. In their work on growth rates of slantwise convection, they obtained a doubling time for CSI on the order of a couple of hours. Subsequently, Bennetts and Sharp (1982) directly applied the relevance of CSI to the prediction of frontal rainbands by utilizing σ^2 for small amplitude disturbances:

$$\sigma^2 = -f\eta_g - \frac{RT}{p\theta_o}\frac{\left(\nabla_h\theta \bullet \nabla_h\theta_w\right)}{\frac{\partial\theta_w}{\partial p}}, \qquad (1)$$

in which θ_o is a reference potential temperature (283 K), θ_w is the wet bulb potential temperature, and the remaining variables take on their usual meteorological meanings. Units for σ^2 are in terms of h^{-2}, with positive (negative) values expected to indicate growth (decay) of the instability. Bennetts and Sharp (1982) found that the growth rate parameter was more useful in the prediction of banded precipitation than in identifying occasions where the rainfall was uniform. In particular, the structure of any frontal precipitation was considered to be almost certainly banded for $\sigma^2 \geq 0.2$ h^{-2}.

An examination of (1) reveals that several constituents contribute to the magnitude and sign of σ^2. Bennetts and Sharp (1982) note that conditions favorable for the development of CSI occur in regions where the two main right-hand-side terms are of similar magnitude. However, a positive value for the growth rate parameter does not necessarily rule out other types of instability (such as conditional instability; CI) nor ensure that the atmosphere is unstable. Consequently, Bennetts and Sharp (1982) advocate that an evaluation of the individual terms in Eq. (1) as well as an analysis of the corresponding synoptic pattern be performed. Without delving into a term-by-term analysis here, σ^2 will be utilized to provide valuable information on the stability tendency of the thundersnow environment.

One technique that has historically been advanced to determine the presence of instability in the atmosphere has been the identification of regions where the moist geostrophic potential vorticity (MPV_g) is less than zero (Schultz and Schumacher 1999; and references therein). It should be noted that (1) is an alternate, but still useful, form of the original theoretical development by Bennetts and Hoskins (1979), which represented the ratio of the wet-bulb potential vorticity to the moist static stability. Although, (1) relies heavily on θ_w, the equivalent potential temperature (θ_e) can easily be substituted in an atmosphere approaching saturation without entailing much variation. Given that many researchers (e.g., Emanuel 1983; Sanders and Bosart 1985; Moore and Lambert 1993; McCann 1995; Nicosia and Grumm 1999; Clark et al. 2002; Jurewicz and Evans 2004; Moore et al. 2005) have employed the latter and diagnosed EPV, this study follows suit. Moreover, the three dimensional vector representation of EPV ($q_e \equiv -g\vartheta_g \bullet \nabla\theta_e$) can be simplified by neglecting the vertical velocity terms and coriolis term in the along-shear direction. By applying these approximations and carrying out the dot product, McCann (1995) obtained:

$$q_e = g\left(\frac{\partial\theta_e}{\partial x}\frac{\partial v_g}{\partial p} - \frac{\partial\theta_e}{\partial y}\frac{\partial u_g}{\partial p} - \frac{\partial v_g}{\partial x} - \left(\frac{\partial u_g}{\partial y} + f\right)\frac{\partial\theta_e}{\partial p}\right), \qquad (2)$$

wherein computations can be easily obtained from gridded data in numerical weather models. Negative values of EPV, in themselves, are necessary but not sufficient for convection to develop. Rather, the ingredients based methodology (Johns and Doswell 1992; Schultz and Schumacher 1999) also requires both a forcing mechanism to lift air parcels as well as ample amounts of moisture for the release of either CI or CSI to occur.

Trends in other commonly diagnosed stability indices could also aid in effectively substantiating the results obtained via (1) and (2). Market et al. (2006) analyzed parameters derived from proximity soundings associated with both thundering and non-thundering snowstorms. A select set of standard stability indices were tested to find specific metrics that would be statistically significant discriminators for the presence of lightning. Results showed that distinct differences existed in the mid-level (700-500hPa) lapse rates, wherein temperatures typically decreased more rapidly for thundersnow events ($6.5\pm1.3 Kkm^{-1}$) compared to non-thundersnow episodes ($5.5\pm0.7 Kkm^{-1}$) at a confidence level of $p = 0.03$. Given this proven means of establishing a relatively less stable regime in cases of snow and lightning, trends in the mid-level lapse rates will be offered for comparison against σ^2 immediately leading up to convective initiation.

3. METHODOLOGY

3.1 Identification of Thundering Snowstorms

METAR and SPECI observations from surface weather stations across the United States were scanned routinely during the winter months (October-April) of 2003-04 and 2004-05. In order to document the occurrence of thundersnow during this time period, reports of thunder with various intensities of snowfall (SN) were counted, such that the lightning was either observed near the surface station (TSSN or VCTSSN) or at some distance away (LTG DSNT). From this dataset, only events associated with an extratropical cyclone (ETC) occurring in the region between the Rocky and Appalachian Mountain ranges (i.e., the central part of the country) were investigated further. Following the methodology applied in Market et al. (2002), twenty-nine separate case studies with corresponding initiation sites were identified by employing an appropriate temporal and spatial criterion for mesoscale processes. Specifically, the identification of distinct convective snow events was accomplished by checking whether either of the two following conditions was met: the separation distance at *different* stations for simultaneous thundersnow reports had to be more than 1100 km or more than 6 hours had to pass with consecutive reports at the *same* station. This procedure was selected by Market et al. (2002) as a reasonable means of discriminating TSSN episodes given the sufficiently unique characteristics of the individual flow regimes.

In order to further substantiate the existence of thundersnow in these case studies, cloud-to-ground (CG) lightning flash data were obtained from the National Lightning Detection Network (NLDN). While a large portion of the lightning that results from cold season, elevated convection is intracloud, Smith et al. (2005) utilized the NLDN as a means to provide additional, solid evidence that electrical activity occurred within half of the archived snowstorms from the 2003-04 season. Furthermore, a more accurate identification of initiation was determined at times by plotting CG-lightning flashes from the NLDN in conjunction with surface weather conditions from nearby METARs, despite that fact that a report of thundersnow was lacking from the individual observations. This methodology helped to obtain additional precision in determining the location and onset of convective snowfall, something which Smith et al. (2005) emphasizes would be important to operational forecasters and their capacity to notify the general public in a timely manner of approaching hazardous weather. By applying this evaluation scheme to the current work, results from this examination will be specifically restricted to the seventeen selected thundersnow cases given in Table 1, these being episodes where lightning flashes could be verified from the NLDN (one event was left out

due to the relatively low amount of moisture present in the sounding profile since the growth rates would require near-saturated conditions).

Table 1. Information on subset of convective snow case studies examined. Location of thundersnow onset is given along with surface weather station identifier when possible. Onset time indicates year, month, date, and closest hour (UTC) for which the first report occurred. As described in the text, the level with the highest significant growth rates [LHSGR(hPa)] is determined for each event at initiation as well as 3-hours prior

TSSN Onset Location	Onset Time	LHSGR(hPa) (Onset, Prior)
Salina, KS (KSLN)	0400 UTC 11-23-2003	(700,800)
Beatrice, NE (KBIE)	1500 UTC 12-09-2003	(600,700)
Tulsa, OK (KRVS)	0400 UTC 12-10-2003	(600,800)
Marion, IL (KMWA)	0400 UTC 01-27-2004	(750,None)
Mountain Home, AR (KBPK)	0300 UTC 02-05-2004	(550,600)
Near Eau Claire, WI (44.6N;90.9W)	0700 UTC 03-05-2004	(550,650)
Hutchinson, MN (KHCD)	1300 UTC 03-13-2004	(700,550)
Amarillo, Texas (KAMA)	0900 UTC 11-02-2004	(550,600)
Kansas City, MO (KMKC)	0700 UTC 11-24-2004	(650,700)
Cape Girardeau, MO (KCGI)	0900 UTC 12-22-2004	(600,550)
Owensboro/Davies, KY (KOWB)	0200 UTC 12-23-2004	(800,800)
Near Watertown, SD (45.1N;96.9W)	1600 UTC 01-01-2005	(700,600)
Near Terre Haute, IN (39.88N;87.26W)	0600 UTC 01-08-2005	(550,550)
Lincoln, IL (KAAA)	0800 UTC 01-22-2005	(650,750)
Benton Harbor, MI (KBEH)	1700 UTC 02-20-2005	(600,800)
Near Albert Lea, MN (43.5N;92.45W)	1100 UTC 03-18-2005	(550,550)
Goodland, KS (KGLD)	0400 UTC 04-11-2005	(700,750)

3.2 Analysis Routine

Mid-level lapse rates and each of the right-hand-side terms in Eqns. (1) and (2) were calculated utilizing the GEneral Meteorological PAcKage (GEMPAK; desJardins et al. 1991) software, with the initial analysis from a 40-km Rapid Update Cycle (RUC-2) model grid providing the necessary input data. Calculations were performed every 50-hPa in the model from 950-hPa to 550-hPa and second-order finite differencing was utilized to evaluate vertical derivatives. Application of the geostrophic wind at such a fine resolution is most likely not appropriate. Thus, a simple Gaussian filter was applied to significantly damp artificial structures at the shortest wavelengths in the raw fields while still retaining true small-scale features. The degree of filtering chosen acted to substantially decrease wave amplitude for length scales below 240-km, thereby mostly eliminating information that would be considered noise in an atmosphere that is in approximate geostrophic balance. Comparison of results in (1) and (2) against observational evidence was accomplished from analyzing basic fields (e.g., heights, winds, temperature) from the RUC-2 analyses and individual (composite) reflectivity patterns from the Next Generation Radar (NEXRAD) level II (level III) radar data.

The RUC-2 numerical model (Benjamin et al. 1998) is unique in its frequent hourly assimilation of the most recent observations, thus providing valuable short-range forecasts and ensuring better confidence when monitoring current conditions. This advantage is important in examining and noting short-term trends in stability characteristics of thundersnow events, especially considering that such phenomena have horizontal dimensions in the meso-β scale range and typically exhibit a timescale on the order of just a few hours (e.g., Emanuel 1986; Market et al. 2002). Moreover, Curran and Pearson (1971) noted that traditional indices would often not produce accurate estimates of instability at the time of the proximity sounding given the fact that convection has already begun. As a result, this study not only investigates the time of initiation, but also takes into account preconditioning of the environment three hours beforehand.

In order to remain consistent with Bennetts and Sharp (1982), calculations of σ^2 were initially performed at 700-hPa and considered significant only in regions where the relative humidity (RH) exceeded 80%. This latter criterion was applied to ensure sufficient saturation of the atmosphere, a necessary condition, as mentioned earlier, in diagnosing the presence of CI or CSI. Indeed, a standard RH of 80% represents a saturated condition with respect to ice for temperatures that support dendrite growth (-13 ^{0}C to -18 ^{0}C). However, given the natural variability in synoptic conditions which exist from one case study to the next, evaluating the likelihood of wintertime convection from one set pressure level is not the best approach. For this reason, an alternative technique was pursued by obtaining separate estimates of σ^2 at the level with the highest significant growth rates (LHSGR) present, which ordinarily was different than 700-hPa. In this way, the authors believe that a more plausible measure of the source and nature of elevated thunderstorms would generally be obtained at the elevation experiencing the least resistance to destabilization. One of the criteria for the LHSGR was that the assessment did not begin until above 850-hPa in order to make certain that the analysis was above ground level as well as avoid spurious results near the surface. The use of the word *significance* in the acronym was the final crucial factor and again meant that ample moisture

had to be present for the parcel instability to be realized. The pressure level for the LHSGR three hours before and at the time of initiation is documented in Table 1.

3.3 Identification of Non-Thundering Snowstorms

The combination of surface observations and the NLDN allowed the ability to select snowstorms associated with an ETC *but without* the presence of lightning. The process, established by Smith (2006) and Market et al. (2006), is similar in many respects to determining episodes of thundersnow. The idea was to diminish both orographic and lake-effect influences by restricting the domain to the same interior portion of the country and picking cases that had snowfall accumulations and rates comparable to the convective snow subset in the climatology of Market et al. (2006). More precisely, observed visibility had to be less than or equal to ¼ mile for an extended time frame, such that the midpoint was defined as the time of balloon flight (1200/0000 UTC). Besides the detection of cloud-to-ground flashes from the NLDN, the *absence* of lightning was further bolstered by the fact that human observers were frequently present at the station locations given in Table 2. For the purpose of the current work, the identical set of non-thundersnow (non-TSSN) events decided in Smith (2006) was evaluated. So as to keep differences between TSSN and non-TSSN limited to just physical mechanisms in the atmosphere, the analysis routine is kept consistent. The RUC-2 is relied upon once again for computations and synopses, with the acquisition of σ^2 and 3D-EPV from the 700-hPa level and the LHSGR. Following the format established in Table 1, seven non-TSSN events (encompassing four winter seasons from 2002-2005) are listed in Table 2.

Table 2. Information on subset of non-thundering snow case studies examined. The time given is year, month, date, and hour of the mid-event period. The location is distinguished by station identifier. Similar to Table 1, the level with the highest significant growth rates [LHSGR(hPa)] is determined for each event at the midpoint as well as 3-hours prior.

Non-TSSN Location	Midpoint Time	LHSGR(hPa) (Midpoint, Prior)
Green Bay, WI (KGRB)	1200 UTC 04-02-2002	(700,600)
Springfield, MO (KSGF)	1200 UTC 01-16-2003	(750,800)
Omaha/Eppley, NE (KOMA)	1200 UTC 02-15-2003	(700,700)
Omaha/Eppley, NE (KOMA)	1200 UTC 03-15-2004	(550,550)
Green Bay, WI (KGRB)	1200 UTC 01-06-2005	(650,550)
Green Bay, WI (KGRB)	1200 UTC 01-22-2005	(800,650)
Green Bay, WI (KGRB)	1200 UTC 02-14-2005	(550,800)

3.4 Approach

The examination of stability characteristics will be pursued in two different fashions. The first will be more quantitative and entail compiling averages and standard deviations for point values of all stability parameters in each case study. To be more precise, these statistics are derived from the individual initiation (TSSN) or midpoint (non-TSSN) sites. Since each station identifier or pair of latitude and longitude (Tables 1 and 2) demarks a specific position not exactly matching the grid points in the RUC-2 model, significance of the results is limited to some extent by the utilization of bilinear interpolation.

Other than the tabular approach, results are also presented through showing plots of atmospheric properties, whether they are directly observed or indirectly derived. Instead of inspecting each case study individually for this objective, discrete spatial composites are produced for both TSSN and non-TSSN situations through means of a moving grid. The size of the sub-domain (31 x 31 grid points) in this study was sufficiently large (1200 km) to capture the background (meso-α to synoptic-scale) aspects associated with both types of snowstorms. Seeing that the origin in the spatial framework has been known to track many analyzed meteorological phenomenon (e.g., Mote et al. 1997; Moore et al. 2003; Oravetz 2003), the scheme here establishes two separate storm-relative composites by centering on the initiation sites of TSSN (Table 1) in one and the midpoint locations for non-TSSN (Table 2) in the other, where the *nearest* grid point in the RUC-2 model represented the centroid. It should be stressed that calculation of derived parameters [like (1) and (2)] occurred before compositing for the strict intention to avoid additional, artificial smoothing in creating averaged fields.

4. RESULTS

4.1 Statistical Findings

Reflectivity data with the best resolution available (most often 1 km; obtained from http://hurricane.ncdc.noaa.gov/pls/plhas/has.dsselect) were examined fromWSR-88D radar stations in each of the TSSN events listed in Table 1. Only the 5 March 2004 case study presented a scenario where no suitably close level II radar data were available, so the more coarse 6 km level III composite information was evaluated instead utilizing GEMPAK. The typical range in LHSGR for TSSN and non-TSSN was estimated from the separate lists of corresponding events. Regardless of the time period examined, a comparison between the two in Table 3 revealed comparable results. The pressure level often varied between 550-700-hPa in each dataset, with

the mean at a slightly higher elevation at initiation in TSSN-events (635-hPa) compared to the midpoint of non-TSSN case studies (671-hPa). Nevertheless, the main aspect that needs to be emphasized is that the vertical location of the best growth rates was found to fluctuate (Table 3).

An initial inspection of the stability tendencies from σ^2 reveals considerable variations in both sign and magnitude from one convective snow episode to another. The progression and sometimes intensification of already robust radar reflectivity returns (usually > 30 dBZ) into the area of interest corroborated the nowcast that wintertime convection might transpire in the near future. This increase in intensity is further supported by the upward trend in average values for σ^2 compiled in Table 4, when comparing the time the event commenced to that from three hours prior, regardless of whether the conventional method advocated by Bennetts and Sharp (1982) or the application of the LHGSR was applied. When making a distinction between the two approaches, however, a more accurate portrayal for susceptibility of the atmosphere to slantwise or upright displacements was not always found at one level. Rather, more favorable conditions were obtained from greater destabilization values for both time periods at the LHSGR (compare Table 4a to 4b), which was typically close to the 650-hPa level (Table 3).

Table 3. Statistics of the LHSGR(hPa) in TSSN and non-TSSN events for the two time periods utilized, such that μ (s) represents the average (standard deviation).

LHSGR(hPa)	Initiation/ Midpoint	Prior
TSSN	635 (79)	672 (102)
Non-TSSN	671 (95)	664 (107)

Table 4. Statistics of σ^2 (h^{-2}) and 3-D EPV ($10^{-6}Kkg^{-1}m^2s^{-1}$) in TSSN events at the (a) 700-hPa level and (b) LHSGR for the two time periods utilized, such that μ (s) represents the average (standard deviation).

(a)

700-hPa	Initiation	Prior
σ^2 (h^{-2})	0.01 (0.33)	-0.43 (1.16)
3-D EPV ($10^{-6}Kkg^{-1}m^2s^{-1}$)	0.46 (0.77)	0.25 (0.49)

(b)

LHSGR(hPa)	Initiation	Prior
σ^2 (h^{-2})	0.30 (0.59)	-0.01 (0.12)
3-D EPV ($10^{-6}Kkg^{-1}m^2s^{-1}$)	-0.03 (0.25)	0.26 (0.65)

More formal support for this conclusion was reached by computations of 3-D EPV (McCann 1995), the statistical results of which are also shown in Table 4. Although a substantial number of the TSSN cases exhibited evidence of weak stability to instability within the vertical profiles, the averages and large standard deviations for 3-D EPV showed that values varied substantially (Table 4). Again, results from this metric revealed that less opposition (i.e., slightly positive to negative estimates) to elevated thunderstorm development was offered at the LHSGR. Along these lines, average values for σ^2 at the time of initiation increased from -0.01 h^{-2} to 0.30 h^{-2} when the more novel approach was used (Table 4b). This latter value corresponds to a σ equal to 0.55 h^{-1} or a doubling time for the disturbance every 1.8 hours, which is approximately consistent with the established time scale (f^{-1}) for moist slantwise convection generated from the release of CSI (e.g., Bennetts and Hoskins 1979; Emanuel 1986).

Table 5 shows similar list of parameters but for the alternate group of non-TSSN events. Characteristic results of σ^2 (3-D EPV) increased (decreased) over the three hour period ending at the midpoint for both the 700-hPa level (Table 5a) and the LHSGR (Table 5b). The latter method was once again associated with relatively reduced stability and elevated growth rates over the former. As was the scenario for TSSN, a large range in values is evident in Table 5 as standard deviations were about on the same order as the averages. Despite this resemblance, the obvious distinction is the larger 3-D EPV and smaller σ^2 statistics in winter storms lacking CG-lightning (contrast Tables 4 and 5). In fact, an evaluation of Eqns. [1] and [2] in Table 5b (-0.06±0.11 h^{-2} and 0.24±0.39 $10^{-6}Kkg^{-1}m^2s^{-1}$) versus that of Table 4b (0.30±0.59 h^{-2} and -0.03±0.25 $10^{-6}Kkg^{-1}m^2s^{-1}$) indicates that the signs for the left-hand-side expressions at the LHSGR and the later time period had a tendency to be opposite to those for TSSN. As a result, the correlation between the two datasets advanced some evidence that instability and destabilization of the environment was more prevalent for instances of cold-season moist convection.

Table 5. Same as in Table 4 except for non-TSSN events.

(a)

700-hPa	Midpoint	Prior
σ^2 (h^{-2})	-0.11 (0.11)	-0.13 (0.09)
3-D EPV ($10^{-6}Kkg^{-1}m^2s^{-1}$)	0.72 (0.71)	0.84 (0.61)

(b)

LHSGR(hPa)	Midpoint	Prior
σ^2 (h^{-2})	-0.06 (0.11)	-0.08 (0.11)
3-D EPV ($10^{-6}Kkg^{-1}m^2s^{-1}$)	0.24 (0.39)	0.53 (0.58)

Standard mid-level (700-500-hPa) lapse rates are presented in Table 6 for both types of snowstorms. Minimal changes in this traditional stability index were noted over the short time frame. For observations of

snow *with* lightning, the temperature drop with height often approached moist adiabatic (approximately 6.5 ^{0}C km^{-1}), this finding being consistent with the 30-year climatology developed by Market et al. (2006). Furthermore, the corresponding collection of non-TSSN lapse rates indicated averages that were slightly more than 1 ^{0}C km^{-1} lower (Table 6). As would be expected, parcels under such atmospheric conditions would be more resistant to the intensification of updrafts. In this respect, the evaluation here aids in supporting stability characteristics from EPV computations. Given the reality that finite and instantaneous trends are not exactly equivalent quantities, suitable testing of the results from σ^2 might not be possible here. Still, the frequent, nearly zero growth rates (Tables 4 and 5) at three hours prior does corresponds somewhat to the approximately static mid-level lapse rates observed (Table 6).

Table 6. Statistics of mid-level (700-500-hPa) lapse rates (^{0}C km^{-1}) in TSSN and non-TSSN events for the two time periods utilized, such that μ (s) represents the average (standard deviation).

Lapse rates (^{0}C km^{-1})	Initiation/ Midpoint	Prior
TSSN	6.2 (0.9)	6.3 (0.9)
Non-TSSN	4.9 (1.5)	4.8 (1.4)

4.2 Composite Analyses

The composite plots produced here complemented the profile results from a single location. The analyses offered a way to inspect the spatial distribution of stability characteristics and visually track their movement with respect to the most intensive part of the snowstorm (whether or not lightning was present). Averages of σ^2 (h^{-2}) and 3-D EPV (10^{-6}Kkg^{-1}m^{2}s^{-1}) are obtained for each grid point in the smaller domain and combined together to refine the forecast area deemed susceptible to convective development. Since the mean pressure level for the LHSGR (Table 3) was not a standard 50-hPa increment as in a weather model, the closest approximation for both datasets and time periods was determined to be 650-hPa for the composites. Finally, the background maps are shown as reference only and at best symbolize the representative area of interest for the case studies.

Figure 1 shows σ^2, 3-D EPV, and RH calculated from the RUC-2 model for the set of previously identified convective snow case studies in this study. The smoothed fields show a small area of instability along the southern border that expands a little northward by the time the first CG-lightning occurs. A larger, surrounding region of slightly stable conditions extends farther into the polar airmass and near the TSSN initiation site. This information is revealed by the orange (red) shaded extent of 3-D EPV values of less than 0.25 (less than zero). The release of either CI or CSI is permitted given the collocation of a nearly saturated atmosphere. While there are some variations in the 3D-EPV pattern dependent upon time frame or pressure level selected, the contoured plots of growth rates vary much more. Pockets of higher, positive σ^2 propagate closer to the centroid over the course of the three hours, with the LL and LR panels in Fig. 1 indicating that the LHSGR exhibits the most favorable increase in values. Consequently, as would be expected, the typical atmosphere near thunderstorm development in winter precipitation events is one that shows signs of destabilization.

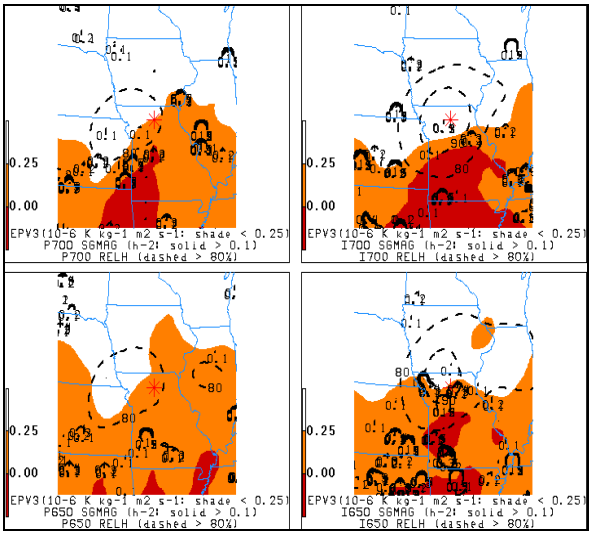

Figure 1. Spatial average composites of σ^2 (h^{-2}; solid lines > 0.1), 3-D EPV (10^{-6}Kkg^{-1}m^{2}s^{-1}; orange shading < 0.25 and red shading <0), and RH (dashed lines > 80%) for the TSSN events compiled. The upper-right (UR) and lower-right (LR) panels represent the time of initiation, whereas the upper-left (UL) and lower-left (LL) panels represent three hours prior. Plots at the 700-hPa level (UL, UR) and the LHSGR (~650-hPa; LL, LR) are presented. The background map is utilized as reference only and the asterisk denotes the approximate position for the average (or typical) TSSN initiation site.

The similarity in synoptic-scale features (e.g., transient ETC) for both sets of winter precipitation events meant that the necessary dynamic and thermodynamic forcing mechanisms are present in either case (not shown). In order to effectively identify discrepancies, other ingredient factors for thunderstorm development must be considered. For this purpose, composites for non-TSSN events are displayed in Fig. 2. Zones of σ^2 greater than zero are displaced farther equatorward compared to Fig. 1, with the lower 3D-EPV estimates not as evident within the domain. Although high RH values near the midpoint site suggest an atmosphere saturated enough for the production of precipitation, these plots indicate the stability regime is insufficient for the development of moist convection in the snowstorm (Fig. 2). The diagnosis reached through

these spatial examinations was also evaluated by fields of mid-level lapse rates (not shown). The resulting analysis further bolstered the uniqueness of and difference between those snowstorms featuring lightning from those that do not.

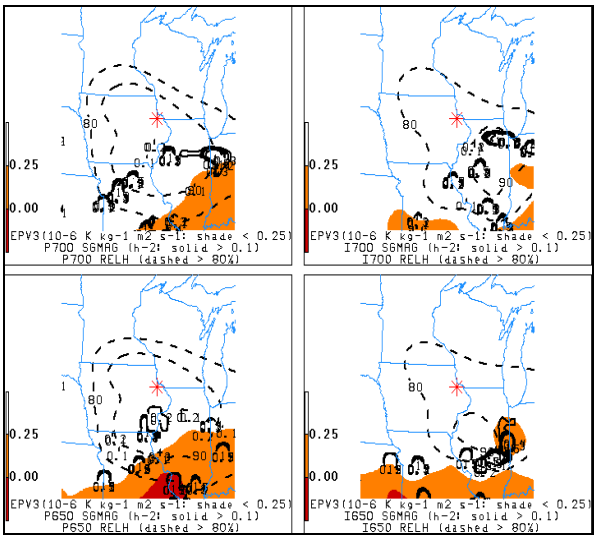

Figure 2. Same as in Fig. 1 except for non-TSSN events compiled. The asterisk denotes the approximate position for the average (or typical) non-TSSN midpoint site.

5. SUMMARY AND CONCLUSIONS

Throughout the current investigation, the main goal was to make a detailed examination of σ^2 for instances of TSSN immediately leading up to the onset of convection. Although modeling and observation studies in Bennetts and Hoskins (1979) and Bennetts and Sharp (1982), respectively, introduced growth rates as a technique for diagnosing CSI, little work has been forthcoming in recent years in the United States. Insights into stability characteristics associated with wintertime, elevated thunderstorms are explored for two seasons and a group of non-TSSN episodes were obtained to stress the findings from σ^2. The inclusion of mid-level lapse rates and 3D-EPV played a complementary part to describing atmospheric conditions and substantiating the results established on this seldom utilized stability parameter.

Upon comparison against the observational evidence (METARs, NLDN, radar reflectivity), this work showed that, on average, σ^2 was very useful in accurately anticipating the expected destabilization of the atmospheric environment immediately leading up to the beginning of lightning activity. Through approaches that entail statistical means and composite graphs of growth rates, greater success was found in obtaining estimates at the LHSGR. This selection was physically more reasonable compared to restricting the analysis to one level in all the thundersnow events since a more ideal situation for convective development is usually where the least resistance to convection is observed.

Unlike Bennetts and Sharp (1982), the lower number of events available to examine here demand caution and permit formulation of only broad guidelines for operational use. For example, the relatively high values for the standard deviation for both σ^2 and 3D-EPV in Table 4 would tend to indicate large differences in conditions for the small sample size. Still, negative (positive) values of the former (latter) parameter occurred at initiation only five times when evaluated from the LHSGR (not shown). In addition, the corresponding magnitudes were often small, thereby keeping resistance to convection at a minimum. The other ingredients for thunderstorms, a nearly saturated environment and robust dynamics to produce updrafts, were present in all TSSN (and for that matter non-TSSN) events. Given the repeated correlations and similarities noted from the current investigation, the usefulness of σ^2 could be more thoroughly measured by comparing plots of the prognostic parameter against plan view radar analyses as well as other observational networks.

One of the main conclusions reached here follows that of Market et al. (2006), in which the diagnostics imply an environment less resistant to upward motions in occurrences of TSSN compared to an otherwise comparable collection of non-TSSN events. Moreover, the analysis approaches revealed a relatively less stable regime that was more prone to destabilization in cases when lightning was present. Some of the techniques employed by this work could be useful for routine implementation in an operational environment. Since significant wintertime weather can often result in hazardous traveling conditions, more precise and accurate means of such events are always needed by forecasters. Similar to what was recommended by Bennetts and Sharp (1982), σ^2 could be computed easily using simple scripts with output generated from fine resolution models. Further, by combining the growth rates with other measures of stability (such as 3D-EPV), the areal extent and temporal duration of potential elevated convection could be narrowed down. This would hopefully provide another tool to help forecasters in predicting the potential for thunderstorm development and the associated, greater precipitation rates and amounts.

Acknowledgements The paper presented here is part of the doctoral work that the primary author is completing while at the University of Missouri-Columbia. This work is supported by the National Science Foundation (NSF), Award No. ATM-0239010. Any opinions, findings, conclusions or recommendations expressed herein are those of the author(s) and do not necessarily reflect the views of NSF.

REFERENCES

Benjamin, S.G., J.M. Brown, K.J. Brundage, B.E. Schwartz, T.G. Smirnova, T.L. Smith and L.L. Morone, 1998: RUC-2 – The Rapid Update Cycle Version 2. NWS Technical Procedures Bulletin No. 448. NOAA/NWS, 18 pp. [Available online at: http://205.156.54.206/om/tpb/448.htm].

Bennetts, D.A., and B.J. Hoskins, 1979: Conditional symmetric instability – a possible explanation for frontal rainbands. *Quart. J. Roy. Meteor. Soc.,* **105,** 945-962.

_____, and J.C. Sharp, 1982: The relevance of conditional symmetric instability to the prediction of mesoscale frontal rainbands. *Quart. J. Roy. Meteor. Soc.,* **108,** 595-602.

Clark, J.H.E., R.P. James, and R.H. Grumm, 2002: A reexamination of the mechanisms responsible for banded precipitation. *Mon. Wea. Rev.*, **130**, 3074-3086.

Curran, J.T., and A.D. Pearson, 1971: Proximity soundings for thunderstorms with snow. Preprints, *7th Conf. on Severe Local Storms*, Kansas City, MO, Amer. Meteor. Soc., 118-119.

desJardins, M.L., K.F. Brill, and S.S. Schotz, 1991: Use of GEMPAK on Unix workstations. Preprints, *Seventh International Conf. on Interactive Information and Processing Systems for Meteorology, Oceanography, and Hydrology*, New Orleans, LA, Amer. Meteor. Soc., 449-453.

Emanuel, K.A., 1983: The Lagrangian parcel dynamics of moist symmetric instability. *J. Atmos. Sci.*, **40**, 2368-2376.

_____, 1986: Overview and definition of mesoscale meteorology. *Mesoscale Meteorology and Forecasting,* P.S. Ray, Ed., Amer. Meteor. Soc., 1-17.

Holle, R.L, and J.V. Cortinas, 1998: Thunderstorms observed at surface temperatures near and below freezing across North America. Preprints, *19th Conf. on Severe Local Storms*, Minneapolis, MN, Amer. Meteor. Soc., 705-708.

Johns, R.J., and C.A. Doswell III, 1992: Severe local storms forecasting. *Wea. Forecasting.*, **7**, 588-612.

Jurewicz, M.L., and M.S. Evans, 2004: A comparison of two banded, heavy snowstorms with very different synoptic settings. *Wea. Forecasting*, **19**, 1011-1028.

Market, P.M., C.E. Halcomb, and R.L. Ebert, 2002: A climatology of thundersnow events over the contiguous United States. *Wea. Forecasting*, **17**, 1290-1295.

_____, A.M. Oravetz, D. Gaede, E. Bookbinder, A.R. Lupo, C.J. Melick, L.L. Smith, R. Thomas, R. Redburn, B.P. Pettegrew, and A.E. Becker, 2006: Proximity soundings of thundersnow in the central United States. *J. Geophys. Res.*, **111**, D19208,10.1029/2006JD007061.

McCann, D.W., 1995: Three-dimensional computations of equivalent potential vorticity. *Wea. Forecasting*, **10**, 798-802.

Melick. C.J., L.L. Smith, B.P. Pettegrew, A.E. Becker, P.S. Market, and A.R. Lupo, 2007: Investigation of stability characteristics of cold-season convective precipitation events by utilizing the growth rate parameter. *J. Geophys. Res.*, in submission.

Moore, J.T., and T.E. Lambert, 1993: The use of equivalent potential vorticity to diagnose regions of conditional symmetric instability. *Wea. Forecasting.* **8,** 301-308.

_____, C.E. Graves, S. Ng, and J.L. Smith, 2005: A process-oriented methodology toward understanding the organization of an extensive mesoscale snowband: A diagnostic case study of 4-5 December 1999. *Wea. Forecasting*, **20**, 35-50.

_____, F.H. Glass, C.E. Graves, S.M. Rochette, and M.J. Singer, 2003: The environment of warm-season elevated thunderstorms associated with heavy rainfall over the central United States. *Wea. Forecasting*. **18,** 861-878.

Mote, T.L., D.W. Gamble, S.J. Underwood, and M.L. Bentley, 1997: Synoptic-scale features common to heavy snowstorms in the southeast United States. *Wea. Forecasting*. **12**, 5-23.

Nicosia, D.J. and R.H. Grumm, 1999: Mesoscale band formation in three major northeastern United States snowstorms. *Wea. Forecasting*. **14**, 346-368.

Oravetz, A.M., 2003: Composite analysis of thundersnow events in the central United States. M.S. Thesis, Department of Atmospheric Sciences, University of Missouri-Columbia, Columbia, MO, 120 pp.

Sanders. F., and L.F. Bosart, 1985: Mesoscale structure in the megalopolitan snowstorm of 11-12 February 1983. Part I: Frontogenetical forcing and symmetric instability. *J. Atmos. Sci.*, **42**, 1050-1061.

Schultz, D.M., 1999: Lake-effect snowstorms in northern Utah and western New York with and without lightning. *Wea. Forecasting*, **14**, 1023-1031.

_____, and P.N. Schumacher, 1999: The use and misuse of conditional symmetric instability. *Mon. Wea. Rev.* **127**, 2709-2732.

Smith, L.L., 2006: Investigating stability evolution of snow storms featuring lightning. M.S. Thesis, Department of Soil, Environmental, and Atmospheric Sciences, University of Missouri-Columbia, Columbia, MO, 121 pp.

_____, C.J. Melick, and P.S. Market, 2005: Examination of thundersnow cases in the United States utilizing NLDN data. Preprints, *Conf. on Meteorological Applications of Lightning Data*, San Diego, CA, Amer. Meteor. Soc., CD-ROM, P2.13.